iScience

Article

Osteoclast-derived arachidonic acid triggers dormant lung adenocarcinoma cell activation

Graphical abstract

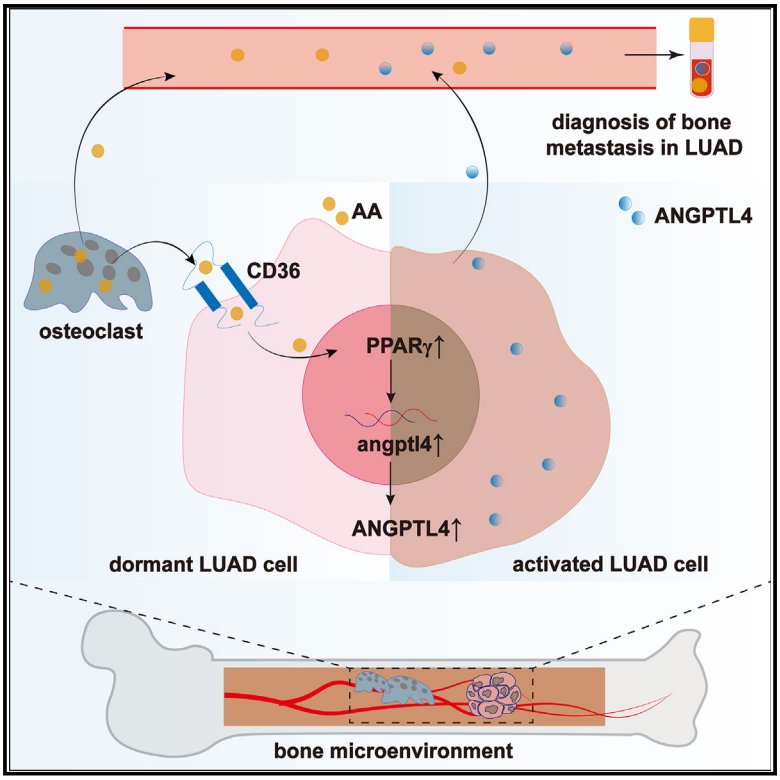

Highlights

- Osteoclast-derived arachidonic acid triggers dormant LUAD activation
- Serum arachidonic acid and ANGPTL4 predict LUAD bone metastasis

Authors

Xingyu Liu, Rong Qiu, Pengcheng Gui, ..., Yingyang Su, Qin Huang, Yuzhen Du

Correspondence

yzdu@sjtu.edu.cn

In brief

Natural sciences; Biological sciences; Biochemistry; Systems biology; Cancer systems biology

Liu et al., 2025, iScience *28*, 112167
May 16, 2025
https://doi.org/10.1016/j.isci.2025.112167

CellPress

iScience

CellPress
OPEN ACCESS

Article

Osteoclast-derived arachidonic acid triggers dormant lung adenocarcinoma cell activation

Xingyu Liu,[1,3] Rong Qiu,[1,3] Pengcheng Gui,[1] Lirong Wei,[1] Yue Lu,[2] Yan Deng,[2] Yang Xue,[1] Yingyang Su,[2] Qin Huang,[1] and Yuzhen Du[1,4,*]

[1]Department of Laboratory Medicine, Shanghai Sixth People's Hospital Affiliated to Shanghai Jiao Tong University School of Medicine, Shanghai, China

[2]College of Fisheries and Life Science, Shanghai Ocean University, Shanghai, China

[3]These authors contributed equally

[4]Lead contact

*Correspondence: yzdu@sjtu.edu.cn

https://doi.org/10.1016/j.isci.2025.112167

SUMMARY

Dormant lung adenocarcinoma (LUAD) cells in the bone microenvironment can re-emerge as metastatic disease through osteoclast interactions. Using a 3D dormancy model and a mouse bone metastasis model, this study reveals that arachidonic acid (AA) is the initiating molecule transferred from osteoclasts to dormant LUAD cells, triggering their activation. Dormant LUAD cells uptake AA through CD36, which activates the PPARγ-ANGPTL4 pathway and activates tumor cells. There is a dose-response relationship in the activation effect of AA, and inhibiting AA metabolism prevents this reactivation. The study also finds that the serum levels of AA and ANGPTL4 are significantly elevated in patients with clinical bone metastases compared to those without. This research confirms that osteoclasts transmit AA via the CD36-PPARγ-ANGPTL4 axis to activate dormant LUAD cells, suggesting that AA and ANGPTL4 may serve as valuable biomarkers and potential clinical applications in treatment and prediction of LUAD bone metastasis.

INTRODUCTION

Lung cancer is one of the leading causes of cancer-related deaths worldwide, with over 90% of patients dying from metastasis-related complications.[1] Lung adenocarcinoma (LUAD) is the most common type of lung cancer, and bone is the most common site of metastasis in LUAD, with an incidence rate of 40%.[2,3] Despite surgical resection being the primary treatment approach, patients may experience recurrent bone metastasis within decades after surgery.[4] This recurrence is closely associated with the dormant state of tumor cells, which reside in the bone microenvironment as low-proliferative single cells or clusters until specific conditions trigger their activation, leading to renewed tumor growth and metastasis.[5] The presence of dormant tumor cells poses a significant challenge in LUAD treatment, and a deeper understanding of the mechanisms that activate these dormant cells could aid in the discovery of new clinical biomarkers and therapeutic targets.

Within the bone microenvironment, the activation of dormant tumor cells is regulated by various factors, among which osteoclasts and osteoblasts are considered key regulators or "switches" of tumor cell activation.[6] Previous findings have shown that LUAD cells can send signals that influence osteoclast activation,[7] and it has been demonstrated that osteoclasts can activate dormant prostate and breast cancer cells through the release of transforming growth factor β (TGF-β) and other factors from the bone matrix via osteolysis.[8,9] However, the specific mechanisms by which activated osteoclasts awaken dormant LUAD cells in bone metastasis remain unclear.

Lipid metabolism, a crucial regulatory mechanism in tumor cells proliferation and migration, has garnered significant attention in recent cancer research.[10] The activation of dormant tumor cells requires energy uptake, and alterations in lipid composition within the tumor microenvironment may influence tumor cells metabolism, thereby influencing the transition between dormancy and activation. For instance, oxidized lipids released during neutrophil stress can activate dormant lung cancer cells[11]; stromal cells in pancreatic cancer can transform into a lipid-rich phenotype, supplying lipids to tumor cells and promoting oxidative phosphorylation, thereby facilitating tumor progression.[12] Beyond serving as "fuel" for cellular growth, lipid molecules also function as signaling molecules between cells.[13] Within the bone microenvironment, the activation of osteoclasts is characterized by significant metabolic alterations, particularly concerning lipid components.[14] Nevertheless, it remains unclear whether the lipid molecules generated during osteoclast activation participate in the transition from dormancy to activation of LUAD cells.

This study investigates the specific mechanisms by which osteoclasts activate dormant LUAD cells, with a focus on lipid metabolism. Osteoclast-derived AA initiated the CD36-PPARγ-ANGPTL4 signaling pathway, ultimately leading to the activation of dormant LUAD cells. Consequently, serum levels of AA and ANGPTL4 are identified as potential early diagnostic biomarkers for LUAD bone metastasis.

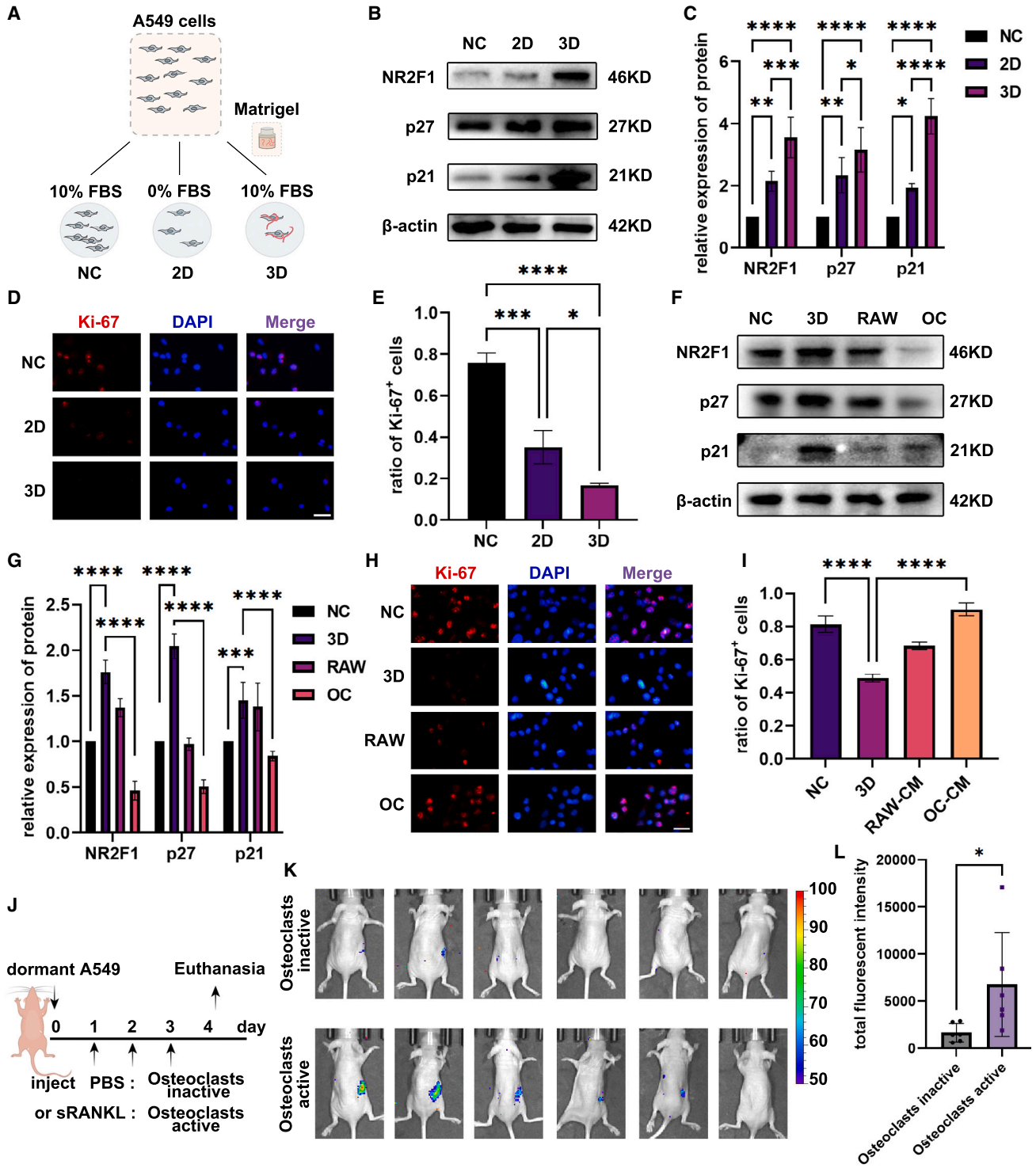

Figure 1. Osteoclast-activated dormant A549 cells *in vivo* and *in vitro*

(A) Schematic diagram of dormancy induction in LUAD cells via serum-free (2D) and matrigel culture (3D).

(B) Western blot (WB) comparison of dormancy marker expression (NR2F1, p27, and p21).

(C) Quantification of dormancy marker expression from (B).

(D) Immunofluorescence (IF) comparison of the proliferation marker Ki-67 expression (scale bars: 25 μm).

(E) Proportion of Ki-67 positive cells from (D).

(legend continued on next page)

RESULTS

Osteoclast activates dormant LUAD cells *in vivo* and *in vitro*

To induce a dormancy state in LUAD cells, both two-dimensional (2D) and three-dimensional (3D) culture systems were employed to replicate the tumor cell dormancy microenvironment (Figures 1A and S1A). After 48 h, an upregulation in the expression of the dormancy marker NR2F1 and the cell-cycle inhibitors p27 and p21 was observed, concomitant with a downregulation in the expression of the proliferation marker Ki-67 (Figures 1B–1E and S1A–S1D). These findings indicate that LUAD cells were successfully induced into a dormancy state, with the 3D culture system demonstrating greater efficacy in promoting this state.

Dormant LUAD cells were treated with conditional medium (CM) from mature osteoclast cultures (OC-CM) for 24 h. After OC-CM treatment, the levels of NR2F1, p21, and p27 in LUAD cells were significantly downregulated, while the Ki-67 positivity rate increased by 40% ($p < 0.001$) (Figures 1F–1I and S1E–S1H), demonstrating that osteoclast-conditioned medium can activate dormant LUAD cells *in vitro* without the need for physical contact. Flow cytometry was used to detect the PI fluorescence intensity of dormant A549 and H1975 cells before and after OC-CM treatment. The results showed that dormant cells were arrested in the G0-G1 phase of the cell cycle without undergoing apoptosis. Upon activation, the proportion of cells in the S phase increased significantly, and the percentage of cells in the G2 phase also rose, indicating that OC-CM activates dormant cells by re-inducing them to enter the S phase. *In vivo* experiments (Figure 1J) revealed that, after tibial injection of dormant A549 cells, five out of six mice subjected to continuous intraperitoneal injection of sRANKL developed overt bone metastases, with the area of bone metastasis lesions larger than in the control group mice (Figures 1K and 1L), indicating that the activation of dormant LUAD cells *in vivo* requires osteoclast activation.

Abnormal PPARγ-ANGPTL4 lipid metabolism pathway is closely related to dormant LUAD cells activation

To investigate the molecular mechanism by which osteoclasts activate dormant LUAD cells, transcriptome sequencing analysis was performed on dormant A549 cells and A549 cells activated by osteoclasts. Focusing on changes in lipid metabolism during the dormancy activation process (Figure 2A), sequencing analysis revealed that by intersecting the differentially expressed genes from transcriptome analysis with lipid metabolism-related gene sets in Kyoto encyclopedia of genes and genomes (KEGG), ANGPTL4 was identified as the most significantly upregulated lipid metabolism-related gene during dormancy activation (fold change ≈25.542) (Figure 2B). Following osteoclast activation, ANGPTL4 expression in LUAD cells was significantly increased at both the mRNA and protein levels ($p < 0.001$) (Figures S2A–S2F), and the concentration of ANGPTL4 in the cell CM was also significantly elevated (Figures 2C and S2G). Using shANGPTL4 to interfere with ANGPTL4 expression in dormant A549 cells and H1975 cells, the activation effect of osteoclasts on dormant cells was inhibited (Figures 2D–2G and S2H–S2K). These findings suggest that osteoclasts can significantly upregulate ANGPTL4 expression in dormant LUAD cells, which is associated with their activation.

To further explore the mechanism by which osteoclasts upregulate ANGPTL4, a protein interaction network analysis was performed, revealing a strong interaction between ANGPTL4 and PPARγ (Figure 2H). PPARγ expression was downregulated in dormant LUAD cells but significantly increased following OC-CM treatment, mirroring the pattern of ANGPTL4 expression (Figures S2A, S2B, and S2D–S2E). The PPARγ inhibitor GW9662 was able to inhibit the activation effect of OC-CM on dormant cells (Figures 2I, 2J, S2L, and S2M), indicating that the PPARγ-ANGPTL4 pathway plays a key role in osteoclast-mediated dormancy activation.

Blocking the lipid uptake channel CD36 inhibits the activation of dormant LUAD cells

The abnormal upregulation of PPARγ-ANGPTL4 suggests activation of lipid metabolism in LUAD cells during dormancy reactivation. PPARγ requires binding with fatty acids taken up by cells to activate. To explore whether the activation of lipid metabolism in dormant cells is related to the transfer of lipid molecules in OC-CM, lipid staining with BODIPY was performed on dormant cells before and after OC-CM treatment. The results showed a significant increase in intracellular lipid content after OC-CM treatment, which was inhibited by the specific inhibitor of the lipid uptake channel CD36, sulfosuccinimidyl oleate (SSO) (Figures 3A, 3B, S3A, and S3B). This suggests that CD36 may play a key regulatory role in lipid metabolism and dormancy activation.

Further validation showed that after treatment with SSO, OC-CM could not upregulate Ki-67 expression (Figures 3C, 3D, S3C, and S3D). The downregulation of dormancy markers was also inhibited (Figures 3E, 3F, S3E, and S3F). These findings indicate that the activation of lipid metabolism in dormant LUAD cells may be related to the uptake of lipid molecules secreted by osteoclasts through the CD36 channel.

(F) WB comparison of dormancy marker expression in A549 cells after 24 h of treatment with CM from RAW264.7 cells and osteoclast cultures.
(G) Quantification of dormancy marker expression from (F).
(H) IF comparison of proliferation marker Ki-67 expression in A549 cells after 24-h treatment with CM from RAW264.7 cells and osteoclast cultures (scale bars: 25 μm).
(I) Proportion of Ki-67 positive cells from (H).
(J) Schematic diagram of the tibial injection model.
(K) Bioluminescence imaging of tibial injection model mice.
(L) Quantification of tumor lesion area in mouse bone. NC: normal control; 2D: serum deprivation-induced dormancy; 3D: Matrigel culture-induced dormancy; RAW: RAW264.7 CM treatment for 24 h; OC: osteoclast CM treatment for 24 h (the statistical data are presented as mean ± SD. (C) and (G) were analyzed using two-way ANOVA, (E) and (I) using one-way ANOVA, and (L) with a two-tailed t test, with multiple comparisons adjusted by Tukey multiple comparisons test. ns: not significant, $^{*}p < 0.05$, $^{**}p < 0.01$, $^{***}p < 0.001$, $^{****}p < 0.0001$.
Also see Figure S1.

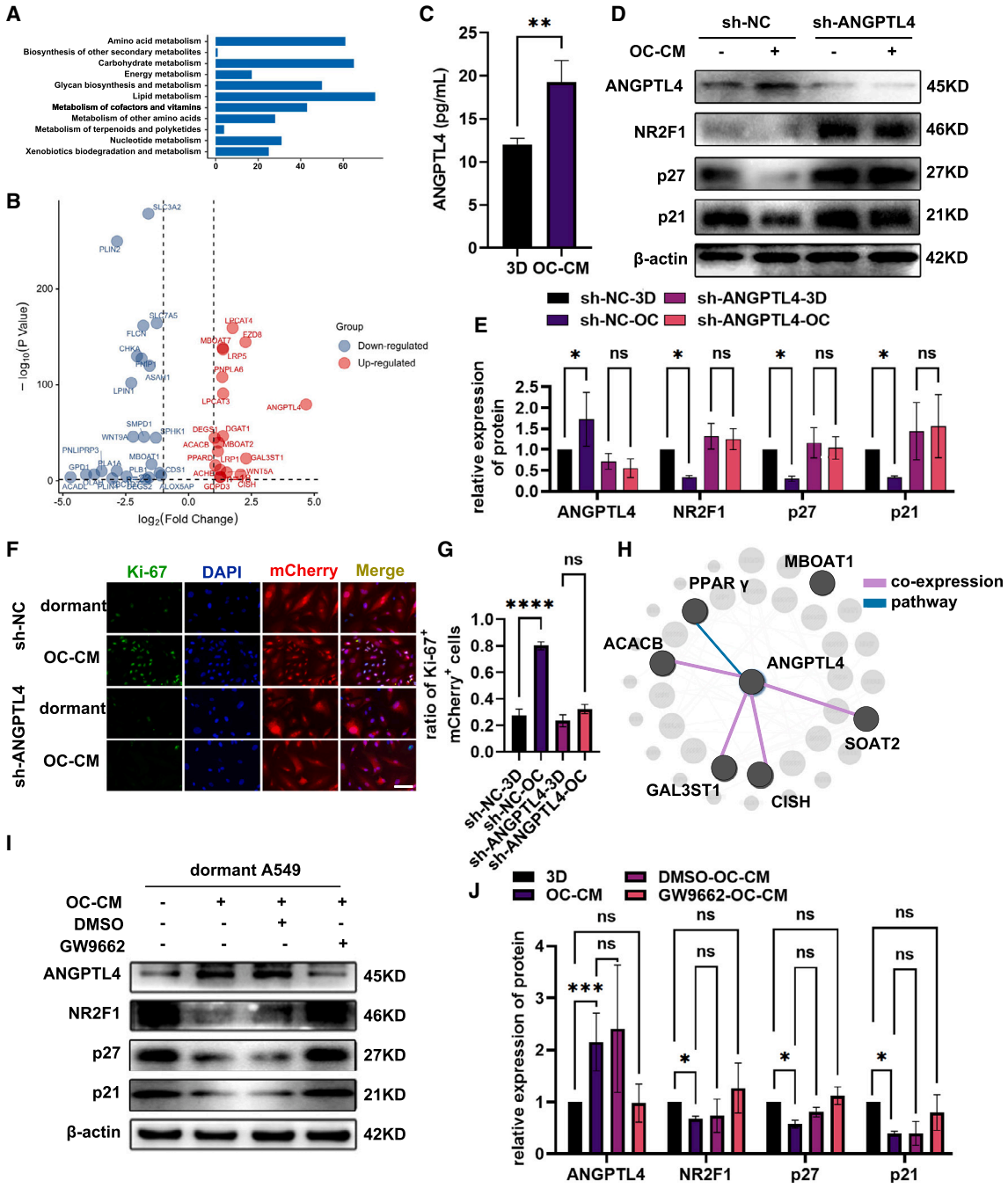

Figure 2. Key role of PPARγ-ANGPTL4 signaling pathway in osteoclast-mediated activation of dormant A549 cells

(A) Enrichment analysis of differentially expressed genes between dormant and activated A549 cells in KEGG metabolism-related pathways.

(B) Volcano plot of differentially expressed genes related to lipid metabolism in dormant A549 cells and osteoclast-activated A549 cells.

(C) ELISA detection of ANGPTL4 expression in the supernatant of dormant A549 cells and osteoclast-activated A549 cells.

(D) WB comparison of the activation effect of OC-CM on dormant A549 cells before and after ANGPTL4 knockdown.

(E) Quantification of dormancy marker and ANGPTL4 expression from (D).

(F) IF comparison of the activation effect of OC-CM on dormant A549 cells before and after ANGPTL4 knockdown (scale bars: 25 μm).

(G) Proportion of mCherry and Ki-67 double-positive cells in (E).

(H) PPI network of upregulated differentially expressed genes.

(I) WB comparison of ANGPTL4 and dormancy marker expression in A549 cells after co-treatment with PPARγ inhibitor GW9662 and OC-CM for 24 h.

(legend continued on next page)

Osteoclast-derived AA is the key lipid molecule in the activation of dormant LUAD cells

Previous studies have found that compared to osteoclast precursor cells RAW264.7, mature osteoclast CM has a significantly higher content of AA and eicosapentaenoic acid(EPA).[15] Purified AA was able to upregulate CD36 expression and mimic the dormancy activation effect of OC-CM, with a dose-response relationship observed in the range of 0.625–5 μM (Figures 4A, 4B, S4A, and S4B). In contrast, EPA did not effectively activate these cells (Figures S4C and S4D). ELISA analysis in this study also showed an increase in AA content in the CM of mature osteoclasts within the osteoclast induction system (Figure 4C). Given the abundant external sources of AA and its inability to be synthesized endogenously, AA cannot be removed from osteoclast CM by inhibiting its synthesis or release. When dormant A549 cells were treated with the AA metabolism inhibitor BW 755C, the activation effect of OC-CM was reduced, as the uptake of AA could no longer be further metabolized (Figures 4D, 4E, S4E, and S4F). In the first part of the study, the serum AA levels in experimental mice were measured. It was found that the serum AA levels in mice with activated osteoclasts were significantly elevated, corresponding to more pronounced tumor foci (Figure S4G). These results confirm that AA plays a crucial role in the activation of dormant LUAD cells.

Upregulation of CD36 and ANGPTL4 is associated with osteoclast-mediated activation of dormant LUAD cells *in vivo*

To validate the aforementioned findings *in vivo*, multiple immunofluorescence staining was performed on the tibiae and femurs of mice with and without distant metastasis, using CK7 as a marker of LUAD cells, and Ki-67 positivity as a marker to distinguish between activated and dormant states. The results indicated that high Ki-67 expression corresponded to larger metastatic lesions, which were accompanied by activated osteoclasts in the surrounding areas (Figures 5A, 5B, and 5D). Conversely, cells in smaller metastatic lesions were more likely to be in a dormant state with low Ki-67 expression (Figures 5A–5C). Correspondingly, in metastatic lesions with low Ki-67 expression, the expression levels of CD36 and ANGPTL4 in LUAD cells were significantly lower than those in lesions with high Ki-67 expression (Figures 5A, 5B, 5E, and 5F). These results *in vivo* confirm that osteoclasts promote the activation and proliferation of dormant LUAD cells by upregulating ANGPTL4 through the lipid uptake channel CD36.

ANGPTL4 and AA are potential biomarkers for bone metastasis in LUAD

In patients with bone metastasis of LUAD, the expression of ANGPTL4 in metastatic sites is significantly higher than in primary sites and is also significantly stronger than in patients with primarytumors (Figure 6A). Data from the cancer genome atlas (TCGA) database show that the progression-free survival of patients with high ANGPTL4 expression (n = 254) is 1.6 years shorter than that of patients with low expression (n = 253) (Figure 6B).

To evaluate the potential clinical diagnostic value of ANGPTL4 and AA, serum samples from LUAD patients were collected and analyzed, with basic clinical information provided in Table S3. ELISA results showed that the serum levels of ANGPTL4 in bone metastasis patients (n = 71) were significantly higher than those in non-metastasis patients (n = 34) ($p < 0.001$), while there was no significant difference between other metastasis patients (n = 40) and non-metastasis patients (Figure 6C). Similarly, the serum AA content in bone metastasis patients (n = 58) was significantly higher than in non-metastasis patients (n = 34) ($p < 0.0001$), with no significant difference between other metastasis patients (n = 31) and non-metastasis patients (Figure 6D).

ROC analysis results indicated that the area under the curve (AUC) for distinguishing non-metastasis and other metastasis from bone metastasis patients was 0.842 for ANGPTL4 (Figure S5A) and 0.855 for AA (Figure S5B), demonstrating their specificity for diagnosing bone metastasis. Since there is a positive correlation between AA and ANGPTL4 (Figure 6E), a combined diagnostic ROC analysis was performed, resulting in an increased AUC value of 0.885 (Figure 6F). These results suggest that ANGPTL4 and AA could serve as potential biomarkers for bone metastasis in LUAD, with a combined diagnostic approach providing better efficacy, and that ANGPTL4 may have value for early diagnosis.

DISCUSSION

LUAD bone metastasis is predominantly osteolytic.[16] During the process of bone metastasis, tumor cells activate osteoclasts, which in turn dissolve bone tissue and release various factors that promote tumor cell proliferation, forming a ‘‘vicious cycle’’.[17] Previous studies have shown that osteoclasts activate dormant breast cancer and prostate cancer cells through growth-promoting molecules such as TGF-β1 and MMP-9 released during bone resorption.[8,18] This study is the first to discover that lipid molecules, specifically AA, secreted by osteoclasts during activation directly activate dormant tumor cells by upregulating PPAR-γ-ANGPTL4 expression in dormant LUAD cells, thereby promoting dormancy activation. Furthermore, elevated levels of AA and ANGPTL4 were detected in the serum of LUAD patients with bone metastasis. This finding provides a new perspective for understanding metabolic reprogramming during the bone metastasis process and offers new targets and biomarkers for early detection and intervention in bone metastasis.

Current research generally suggests that dormant tumor cells have a lower metabolic rate and are less reliant on aerobic respiration, instead depending more on glucose, glutamine, and fatty acid metabolism for energy.[19] Highly proliferative tumor cells

(J) Quantification of ANGPTL4 and dormancy marker expression in (I). NC: normal control; 3D: Matrigel culture-induced dormancy; DMSO: DMSO treatment for 24 h; OC: osteoclast CM treatment for 24 h; GW9662: 10 μM GW9662 treatment for 24 h (the statistical data are presented as mean ± SD. (E) and (J) were analyzed using two-way ANOVA, (G) and (I) using one-way ANOVA, and (C) with a two-tailed t test, with multiple comparisons adjusted by Tukey multiple comparisons test. ns: not significant, *$p < 0.05$, **$p < 0.01$, ***$p < 0.001$, ****$p < 0.0001$.
Also see Figure S2.

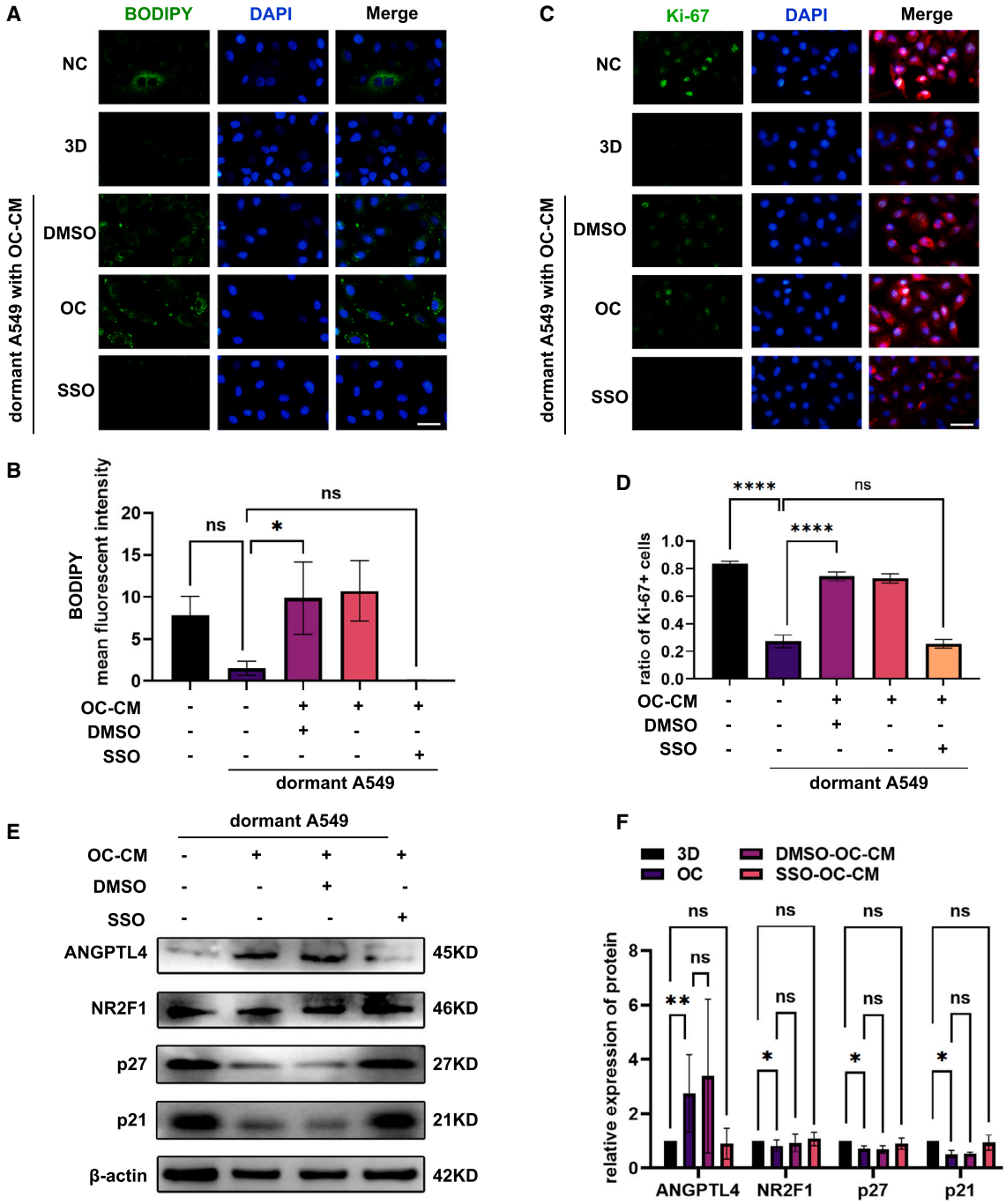

Figure 3. CD36-dependent lipid uptake drives activation of dormant A549 cells

(A) IF comparison of intracellular lipid content in dormant A549 cells after treatment with OC-CM and OC-CM combined with SSO (scale bars: 25 μm).

(B) Quantification of lipid content in (A).

(C) IF comparison of Ki-67 expression in dormant A549 cells after treatment with OC-CM and OC-CM combined with SSO (scale bars: 25 μm).

(D) Quantification of Ki-67 expression in (C).

(E) WB comparison of the expression of ANGPTL4 and dormancy markers in A549 cells after co-treatment with the CD36 inhibitor SSO and OC-CM.

(F) Quantification of ANGPTL4 and dormancy marker expression in (E). NC: normal control; 3D: Matrigel culture-induced dormancy; DMSO: DMSO treatment for 24 h; OC: osteoclast CM treatment for 24 h; SSO: 50 nM SSO treatment for 24 h (the statistical data are presented as mean ± SD. (F) was analyzed using two-way ANOVA, (B) and (D) using one-way ANOVA, and (L) with a two-tailed t test, with multiple comparisons adjusted by Tukey multiple comparisons test. ns: not significant, $*p < 0.05$, $**p < 0.01$, $***p < 0.001$, $****p < 0.0001$.

Also see Figure S3.

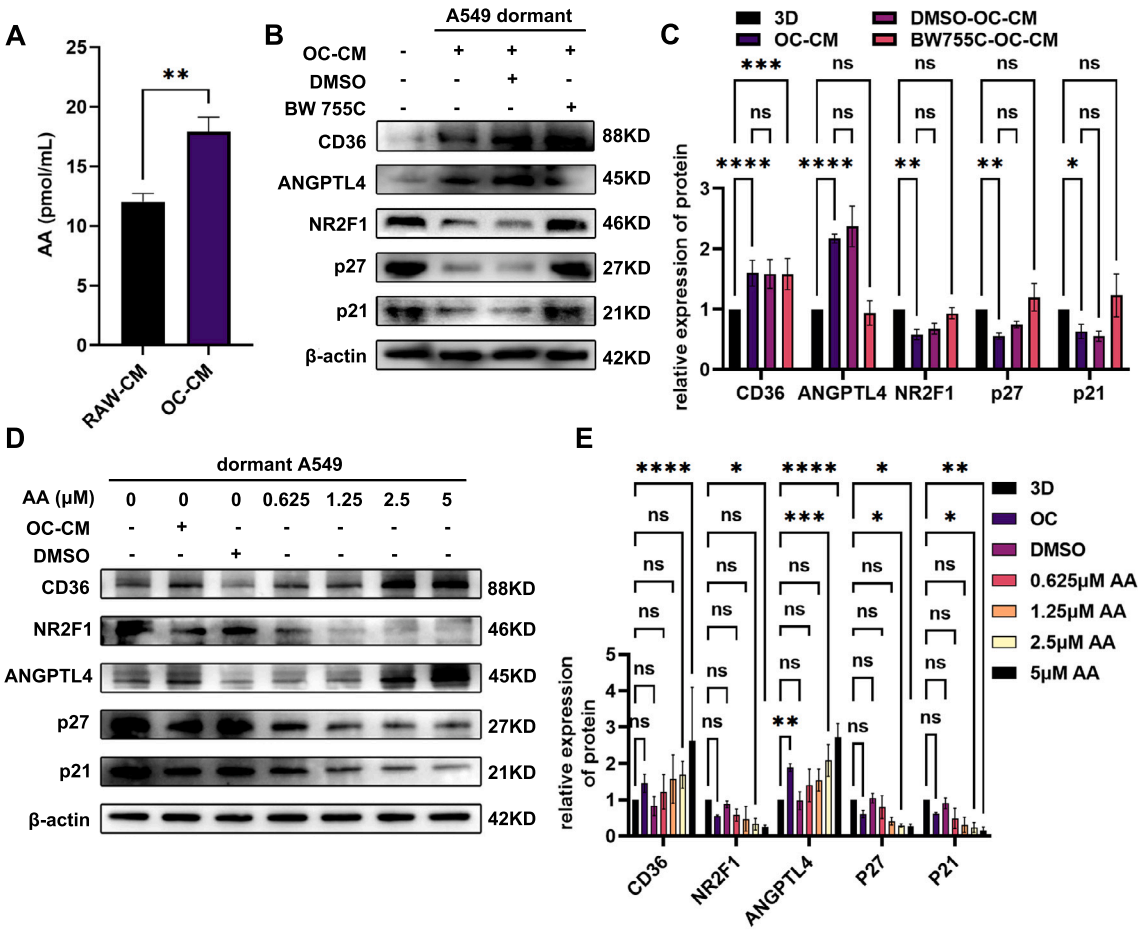

Figure 4. AA from osteoclasts triggers dormant A549 cell activation in a dose-dependent manner

(A) WB analysis of the activation effect of different concentrations of AA (0.625–5 μM) on dormant A549 cells.

(B) Quantification of CD36, ANGPTL4, and dormancy marker expression in (B).

(C) ELISA detection of AA content in the CM of RAW264.7 cells and mature osteoclasts.

(D) WB analysis of the activation effect of OC-CM on dormant A549 cells after treatment with BW 755C.

(E) Quantification of ANGPTL4 and dormancy marker expression in (D). 3D: Matrigel culture-induced dormancy; DMSO: DMSO treatment for 24 h; OC: Osteoclast CM treatment for 24h; AA: 0.625-5 Mm AA treatment for 24 h (The statistical data are presented as mean ± SD. (B) and (E) were analyzed using two-way ANOVA, and (C) with a two-tailed t test, with multiple comparisons adjusted by Tukey multiple comparisons test. ns: not significant, $^{*}p < 0.05$, $^{**}p < 0.01$, $^{***}p < 0.001$, $^{****}p < 0.0001$.

Also see Figure S4.

often exhibit strong lipid affinity.[20] Researchers suggest that lipid accumulation plays a role in dormancy activation, potentially activating dormant tumor cells through the fibroblast growth factor receptor (FGFR) pathway.[11] Lipid-laden macrophages can transfer cholesterol to glioblastoma cells and promote their proliferation.[21] Although the specific lipid components involved are not yet clear, researchers propose the possibility that lipid molecules are key players in dormancy activation. CD36 is a major channel for the entry of free fatty acids into cells, facilitating fatty acid uptake and accumulation to fuel lipid β-oxidation, thereby giving tumor cells a more invasive phenotype.[22] The results of this study suggest that CD36 plays a key role in the activation of bone-metastatic dormant tumor cells. Dormant tumor cells absorb AA transmitted by osteoclasts through CD36 on their membrane and upregulate lipid metabolism-related genes such as PPARγ-ANGPTL4, thereby regaining their rapid proliferation capability. ANGPTL4 was initially identified as a key regulator of triglyceride metabolism.[23] PPARγ is an upstream molecule of ANGPTL4, involved in lipid metabolism, both of which have been reported to be involved in tumor progression. Notably, the effects of PPARγ on tumors are context-dependent. During the early stages of tumorigenesis, PPARγ agonists exhibit tumor-suppressive properties. However, in later stages, particularly during tumor metastasis, PPARγ demonstrates pro-tumor effects. These pro-tumor effects are often associated with metabolic dysregulation or aberrations in specific molecular pathways.[24,25] PPARγ/retinoid X receptor α heterodimer specifically binds to the ANGPTL4 promoter region, thereby enhancing its transcriptional activity.[26] In addition, it has been suggested that ANGPTL4 can activate the PPARγ-Akt pathway.[27] Whether

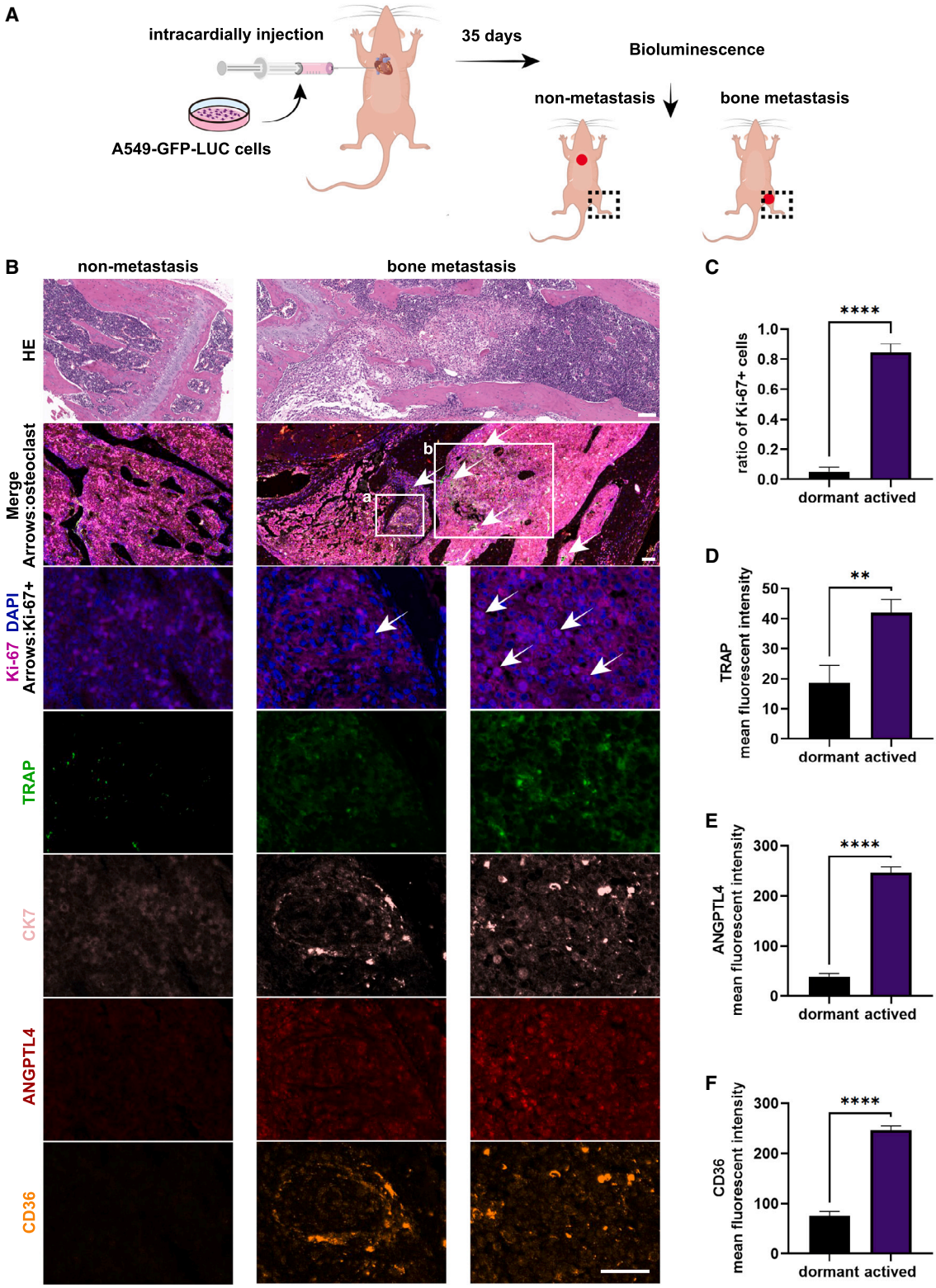

Figure 5. Upregulation of CD36 and ANGPTL4 is associated with osteoclast-mediated activation of dormant LUAD cells *in vivo*

(A) Schematic diagram of the bone metastasis mouse model.

(B) H&E staining and multiplex immunofluorescence detection of Ki-67, TRAP, CK7, ANGPTL4, and CD36 expression in the tibia and femur of mice without metastasis and with bone metastasis (arrows indicate osteoclasts or Ki-67+ cells). a. Dormant lesions (low Ki-67); b. Activated lesions (high Ki-67) (scale bar: 100 μm).

(legend continued on next page)

the PPARγ-ANGPTL4 axis similarly contributes to the activation of dormant tumor cells and subsequently promotes tumor progression warrants further investigation. Transcriptome sequencing results and *in vivo* models support the mechanism by which osteoclasts activate dormant cells through lipid metabolism pathways.

To further identify the key molecules transmitted by osteoclasts, researchers conducted a literature review. Compared to osteoclast precursor cells, the most upregulated lipid molecule in the conditioned medium of mature osteoclasts is AA, which stimulates bone metastasis in breast cancer cells.[15] Since AA is a direct precursor of prostaglandin E2 (PGE2), prostacyclin (PGI2), thromboxane A2 (TXA2), and leukotriene C4 (LTC4), all of which play important regulatory roles in lipid metabolism,[28] and given AA's stronger metastasis-promoting potential compared to other fatty acids, we hypothesize that AA may also play a crucial role in dormancy activation. In this study, inhibiting AA metabolism prevented the absorbed AA from exerting its dormancy activation effect, possibly because it affected the downstream transmission of its metabolites as signaling molecules. Moreover, the *in vitro* application of different concentrations of AA on dormant tumor cells revealed a dose-response relationship in the activation effect of AA, further confirming our hypothesis. We ultimately identified osteoclast-derived AA as the initial molecule triggering dormancy activation. This suggests that AA plays a key role throughout the bone metastasis progression, from promoting migration and invasion to activating dormant cells and enhancing proliferation. Lipids can act as signaling molecules directly influencing tumor cell behavior, enriching the complex interactions between osteoclasts and tumor cells and expanding the value of lipids in the tumor cell life cycle.

The association between a high-fat internal environment and tumor metastasis is widely recognized,[29] and abnormal lipid metabolism may be associated with increased risk of tumor metastasis.[30] Previous studies have found that AA levels increase in mice following osteoclast activation and bone resorption.[15] ANGPTL4, as a downstream molecule in dormancy activation, can inhibit lipid storage and promote lipid breakdown, thereby affecting lipid metabolism in tumor cells.[31] This also suggests that patients with bone metastasis may have abnormal lipid composition in their bodies. Current clinical diagnosis of bone metastasis relies on imaging techniques, which often fail to detect early-stage metastasis until tumor invasion has occurred, limiting early diagnosis and treatment.[32] Previously, our team developed a multi-indicator serum-based prediction model for bone metastasis in non-small cell lung cancer (NSCLC). However, considering the limited interpretability of multi-indicator models, this study aims to explore the diagnostic efficacy of single or dual biomarkers and further investigate the mechanisms underlying bone metastasis in LUAD.[33] Given the key roles of AA and ANGPTL4 in the mechanism of bone metastasis and the urgent clinical need, this study proposes the potential of AA and ANGPTL4 as biomarkers for LUAD bone metastasis. The study found that serum levels of AA and ANGPTL4 in patients with bone metastasis were significantly higher than in those without metastasis and other metastases, with the combined detection achieving good clinical diagnostic performance (AUC = 0.885). This provides strong support for identifying biomarkers for LUAD bone metastasis from a metabolic perspective. Additionally, ANGPTL4 increases peripheral triglyceride levels by inhibiting LPL activity,[34] and its combined detection with other blood lipid indicators, such as triglycerides, could enhance diagnostic specificity and sensitivity.

Our findings suggest that osteoclast-derived AA is the initiating molecule for the activation of dormant LUAD cells. However, the maturation of osteoclasts is accompanied by significant metabolic changes, with multiple lipid molecules being upregulated. Whether AA is the sole lipid molecule involved in this process still requires further investigation. Additionally, AA is absorbed by the CD36 on the membrane surface of dormant LUAD cells; its activation effect can be inhibited by the metabolic inhibitor BW 755C. However, it remains unclear which specific metabolic product is involved in activating PPARγ. Although the potential of AA and ANGPTL4 as biomarkers has been preliminarily suggested, validation with a larger number of clinical samples is still necessary. This study highlights the potential of investigating the mechanisms of dormant tumor cell activation from the perspective of lipid metabolism and provides novel potential therapeutic targets and biomarkers for the early diagnosis of bone metastasis in LUAD.

Limitations of the study

While our findings highlight the role of AA and ANGPTL4 in dormancy activation, the study has limitations. First, the contribution of other osteoclast-derived lipids remains unexplored. Second, the specific AA metabolite responsible for PPARγ activation requires further investigation. Finally, clinical validation of biomarkers needs larger cohorts.

RESOURCE AVAILABILITY

Lead contact

Further information and requests for resources and reagents should be directed to and will be fulfilled by the lead contact, Dr. Yuzhen Du (yzdu@sjtu.edu.cn).

Materials availability

This study did not generate new unique reagents.

Plasmids and/or cell lines generated in this study are available upon reasonable request. Please contact the lead contact.

Data and code availability

RNA-seq data have been deposited at GEO under accession code GEO: GSE289262.

All other data supporting this study are available from the lead contact upon request.

(C) Proportion of Ki-67 positive cells in dormant and activated metastatic lesions.
(D) Average fluorescence intensity of TRAP in dormant and activated metastatic lesions.
(E) Average fluorescence intensity of ANGPTL4 in dormant and activated metastatic lesions.
(F) Average fluorescence intensity of CD36 in dormant and activated metastatic lesions (The statistical data are presented as mean ± SD. (C)–(F) were analyzed using two-tailed t test. $^{**}p < 0.01$, $^{****}p < 0.0001$.

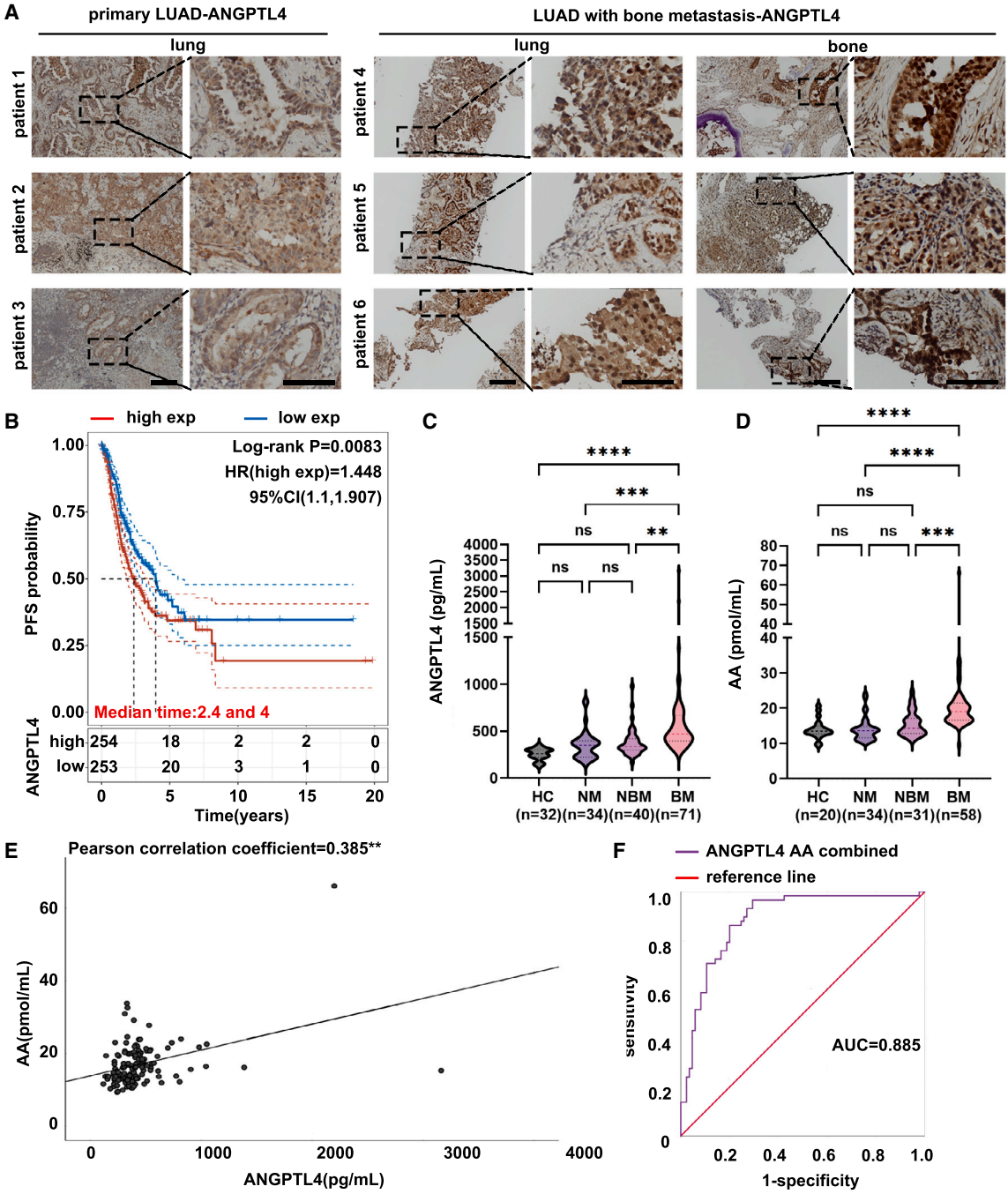

Figure 6. AA and ANGPTL4 identified as potential biomarkers for LUAD bone metastasis diagnosis

(A) Expression levels of ANGPTL4 in different sites of patients with and without bone metastasis in LUAD.

(B) Progression-free survival in patients with high/low ANGPTL4 expression in the TCGA database.

(C) ELISA detection of serum ANGPTL4 levels in LUAD patients without and with bone metastasis.

(D) ELISA detection of serum AA levels in LUAD patients without and with bone metastasis.

(E) Correlation analysis between AA and ANGPTL4.

(F) ROC curve showing the diagnostic value of combined ANGPTL4 and AA in bone metastasis of LUAD (abbreviations: HC, healthy control; NM, non-metastasis; NBM, non-bone metastasis; BM, bone metastasis. Scale bar: left 500 μm, right 100 μm). (The statistical data are presented as mean ± SD. (C) and (D) were analyzed using one-way ANOVA, with multiple comparisons adjusted by Tukey multiple comparisons test. ns: not significant, $^{*}p < 0.05$, $^{**}p < 0.01$, $^{***}p < 0.001$, $^{****}p < 0.0001$.

Also see Figure S5.

ACKNOWLEDGMENTS

This study was financially supported by the National Natural Science Foundation of China (81974315).

AUTHOR CONTRIBUTIONS

X.L., R.Q., P.G., L.W., Y.L., Y.D., Y.X., Y.S., and Q.H. performed the experiments; Y.D. provided materials and expertise; X.L., R.Q., and P.G. designed the experiments, analyzed the data, and wrote the manuscript.

DECLARATION OF INTERESTS

The authors declare no competing interests.

STAR★METHODS

Detailed methods are provided in the online version of this paper and include the following:

- KEY RESOURCES TABLE
- EXPERIMENTAL MODEL AND STUDY PARTICIPANT DETAILS
  - Patients and sample collection
  - Animal experiments
- METHOD DETAILS
  - Bioinformatics analysis
  - Transcriptome sequencing
  - Construction of 3D dormancy model
  - Osteoclast differentiation
  - Cell culture and transfection
  - Quantitative real-time PCR (qRT-PCR) assay
  - Western blot
  - IHC staining
  - ELISA
  - Flow cytometric analysis
  - Immunofluorescence staining
  - Tissue multiplex immunofluorescence staining
- QUANTIFICATION AND STATISTICAL ANALYSIS
- ADDITIONAL RESOURCES

SUPPLEMENTAL INFORMATION

Supplemental information can be found online at https://doi.org/10.1016/j.isci.2025.112167.

Received: October 15, 2024
Revised: January 5, 2025
Accepted: March 3, 2025
Published: March 26, 2025

REFERENCES

1. Sung, H., Ferlay, J., Siegel, R.L., Laversanne, M., Soerjomataram, I., Jemal, A., and Bray, F. (2021). Global Cancer Statistics 2020: GLOBOCAN Estimates of Incidence and Mortality Worldwide for 36 Cancers in 185 Countries. CA Cancer J. Clin. *71*, 209–249. https://doi.org/10.3322/caac.21660.
2. Herbst, R.S., Morgensztern, D., and Boshoff, C. (2018). The biology and management of non-small cell lung cancer. Nature *553*, 446–454. https://doi.org/10.1038/nature25183.
3. Riihimäki, M., Hemminki, A., Fallah, M., Thomsen, H., Sundquist, K., Sundquist, J., and Hemminki, K. (2014). Metastatic sites and survival in lung cancer. Lung Cancer *86*, 78–84. https://doi.org/10.1016/j.lungcan.2014.07.020.
4. Isaka, T., Ito, H., Nakayama, H., Yokose, T., Saito, H., and Masuda, M. (2022). Impact of the initial site of recurrence on prognosis after curative surgery for primary lung cancer. Eur. J. Cardio. Thorac. Surg. *61*, 778–786. https://doi.org/10.1093/ejcts/ezab442.
5. Phan, T.G., and Croucher, P.I. (2020). The dormant cancer cell life cycle. Nat. Rev. Cancer *20*, 398–411. https://doi.org/10.1038/s41568-020-0263-0.
6. Yates, L.R., Knappskog, S., Wedge, D., Farmery, J.H.R., Gonzalez, S., Martincorena, I., Alexandrov, L.B., Van Loo, P., Haugland, H.K., Lilleng, P.K., et al. (2017). Genomic Evolution of Breast Cancer Metastasis and Relapse. Cancer Cell *32*, 169–184.e7. https://doi.org/10.1016/j.ccell.2017.07.005.
7. Yin, J.J., Pollock, C.B., and Kelly, K. (2005). Mechanisms of cancer metastasis to the bone. Cell Res. *15*, 57–62. https://doi.org/10.1038/sj.cr.7290266.
8. Tivari, S., Lu, H., Dasgupta, T., De Lorenzo, M.S., and Wieder, R. (2018). Reawakening of dormant estrogen-dependent human breast cancer cells by bone marrow stroma secretory senescence. Cell Commun. Signal. *16*, 48. https://doi.org/10.1186/s12964-018-0259-5.
9. Ottewell, P.D., Wang, N., Meek, J., Fowles, C.A., Croucher, P.I., Eaton, C.L., and Holen, I. (2014). Castration-induced bone loss triggers growth of disseminated prostate cancer cells in bone. Endocr. Relat. Cancer *21*, 769–781. https://doi.org/10.1530/erc-14-0199.
10. Jin, H.R., Wang, J., Wang, Z.J., Xi, M.J., Xia, B.H., Deng, K., and Yang, J.L. (2023). Lipid metabolic reprogramming in tumor microenvironment: from mechanisms to therapeutics. J. Hematol. Oncol. *16*, 103. https://doi.org/10.1186/s13045-023-01498-2.
11. Perego, M., Tyurin, V.A., Tyurina, Y.Y., Yellets, J., Nacarelli, T., Lin, C., Nefedova, Y., Kossenkov, A., Liu, Q., Sreedhar, S., et al. (2020). Reactivation of dormant tumor cells by modified lipids derived from stress-activated neutrophils. Sci. Transl. Med. *12*, eabb5817. https://doi.org/10.1126/scitranslmed.abb5817.
12. Niu, N., Shen, X., Wang, Z., Chen, Y., Weng, Y., Yu, F., Tang, Y., Lu, P., Liu, M., Wang, L., et al. (2024). Tumor cell-intrinsic epigenetic dysregulation shapes cancer-associated fibroblasts heterogeneity to metabolically support pancreatic cancer. Cancer Cell *42*, 869–884.e9. https://doi.org/10.1016/j.ccell.2024.03.005.
13. Martin-Perez, M., Urdiroz-Urricelqui, U., Bigas, C., and Benitah, S.A. (2022). The role of lipids in cancer progression and metastasis. Cell Metab. *34*, 1675–1699. https://doi.org/10.1016/j.cmet.2022.09.023.
14. Ledesma-Colunga, M.G., Passin, V., Lademann, F., Hofbauer, L.C., and Rauner, M. (2023). Novel Insights into Osteoclast Energy Metabolism. Curr. Osteoporos. Rep. *21*, 660–669. https://doi.org/10.1007/s11914-023-00825-3.
15. Krzeszinski, J.Y., Schwaid, A.G., Cheng, W.Y., Jin, Z., Gallegos, Z.R., Saghatelian, A., and Wan, Y. (2017). Lipid Osteoclastokines Regulate Breast Cancer Bone Metastasis. Endocrinology *158*, 477–489. https://doi.org/10.1210/en.2016-1570.
16. Wu, S., Pan, Y., Mao, Y., Chen, Y., and He, Y. (2021). Current progress and mechanisms of bone metastasis in lung cancer: a narrative review. Transl. Lung Cancer Res. *10*, 439–451. https://doi.org/10.21037/tlcr-20-835.
17. Paget, S. (1989). The distribution of secondary growths in cancer of the breast. 1889. Cancer Metastasis Rev. *8*, 98–101.
18. Albrengues, J., Shields, M.A., Ng, D., Park, C.G., Ambrico, A., Poindexter, M.E., Upadhyay, P., Uyeminami, D.L., Pommier, A., Küttner, V., et al. (2018). Neutrophil extracellular traps produced during inflammation awaken dormant cancer cells in mice. Science *361*, eaao4227. https://doi.org/10.1126/science.aao4227.
19. Huang, B., Song, B.L., and Xu, C. (2020). Cholesterol metabolism in cancer: mechanisms and therapeutic opportunities. Nat. Metab. *2*, 132–141. https://doi.org/10.1038/s42255-020-0174-0.
20. Dai, W., Xiang, W., Han, L., Yuan, Z., Wang, R., Ma, Y., Yang, Y., Cai, S., Xu, Y., Mo, S., et al. (2022). PTPRO represses colorectal cancer tumorigenesis and progression by reprogramming fatty acid metabolism. Cancer Commun. *42*, 848–867. https://doi.org/10.1002/cac2.12341.

21. Kloosterman, D.J., Erbani, J., Boon, M., Farber, M., Handgraaf, S.M., Ando-Kuri, M., Sánchez-López, E., Fontein, B., Mertz, M., Nieuwland, M., et al. (2024). Macrophage-mediated myelin recycling fuels brain cancer malignancy. Cell *187*, 5336–5356.e30. https://doi.org/10.1016/j.cell.2024.07.030.

22. Wang, J., and Li, Y. (2019). CD36 tango in cancer: signaling pathways and functions. Theranostics *9*, 4893–4908. https://doi.org/10.7150/thno.36037.

23. Xu, Z., and Jiang, G. (2024). ANGPTL4-A protein involved in glucose metabolism, lipid metabolism, and tumor development. J. Gene Med. *26*, e3740. https://doi.org/10.1002/jgm.3740.

24. Forootan, F.S., Forootan, S.S., Malki, M.I., Chen, D., Li, G., Lin, K., Rudland, P.S., Foster, C.S., and Ke, Y. (2014). The expression of C-FABP and PPARγ and their prognostic significance in prostate cancer. Int. J. Oncol. *44*, 265–275. https://doi.org/10.3892/ijo.2013.2166.

25. Li, H., Sorenson, A.L., Poczobutt, J., Amin, J., Joyal, T., Sullivan, T., Crossno, J.T., Jr., Weiser-Evans, M.C.M., and Nemenoff, R.A. (2011). Activation of PPARγ in myeloid cells promotes lung cancer progression and metastasis. PLoS One *6*, e28133. https://doi.org/10.1371/journal.pone.0028133.

26. Liu, L., Zhuang, X., Jiang, M., Guan, F., Fu, Q., and Lin, J. (2017). ANGPTL4 mediates the protective role of PPARγ activators in the pathogenesis of preeclampsia. Cell Death Dis. *8*, e3054. https://doi.org/10.1038/cddis.2017.419.

27. Zhu, X., Zhang, X., Gu, W., Zhao, H., Hao, S., and Ning, Z. (2023). ANGPTL4 suppresses the profibrogenic functions of atrial fibroblasts induced by angiotensin II by up-regulating PPARγ. Iran. J. Basic Med. Sci. *26*, 587–593. https://doi.org/10.22038/ijbms.2023.69196.15077.

28. Yarla, N.S., Bishayee, A., Sethi, G., Reddanna, P., Kalle, A.M., Dhananjaya, B.L., Dowluru, K.S.V.G.K., Chintala, R., and Duddukuri, G.R. (2016). Targeting arachidonic acid pathway by natural products for cancer prevention and therapy. Semin. Cancer Biol. *40–41*, 48–81. https://doi.org/10.1016/j.semcancer.2016.02.001.

29. Hursting, S.D., and Dunlap, S.M. (2012). Obesity, metabolic dysregulation, and cancer: a growing concern and an inflammatory (and microenvironmental) issue. Ann. N. Y. Acad. Sci. *1271*, 82–87. https://doi.org/10.1111/j.1749-6632.2012.06737.x.

30. Vogel, F.C.E., Chaves-Filho, A.B., and Schulze, A. (2024). Lipids as mediators of cancer progression and metastasis. Nat. Cancer *5*, 16–29. https://doi.org/10.1038/s43018-023-00702-z.

31. La Paglia, L., Listì, A., Caruso, S., Amodeo, V., Passiglia, F., Bazan, V., and Fanale, D. (2017). Potential Role of ANGPTL4 in the Cross Talk between Metabolism and Cancer through PPAR Signaling Pathway. PPAR Res. *2017*, 8187235. https://doi.org/10.1155/2017/8187235.

32. Peterson, L.M., O'Sullivan, J., Wu, Q.V., Novakova-Jiresova, A., Jenkins, I., Lee, J.H., Shields, A., Montgomery, S., Linden, H.M., Gralow, J., et al. (2018). Prospective Study of Serial (18)F-FDG PET and (18)F-Fluoride PET to Predict Time to Skeletal-Related Events, Time to Progression, and Survival in Patients with Bone-Dominant Metastatic Breast Cancer. J. Nucl. Med. *59*, 1823–1830. https://doi.org/10.2967/jnumed.118.211102.

33. Teng, X., Han, K., Jin, W., Ma, L., Wei, L., Min, D., Chen, L., and Du, Y. (2024). Development and validation of an early diagnosis model for bone metastasis in non-small cell lung cancer based on serological characteristics of the bone metastasis mechanism. EClinicalMedicine *72*, 102617. https://doi.org/10.1016/j.eclinm.2024.102617.

34. Singh, A.K., Chaube, B., Zhang, X., Sun, J., Citrin, K.M., Canfrán-Duque, A., Aryal, B., Rotllan, N., Varela, L., Lee, R.G., et al. (2021). Hepatocyte-specific suppression of ANGPTL4 improves obesity-associated diabetes and mitigates atherosclerosis in mice. J. Clin. Investig. *131*, e140989. https://doi.org/10.1172/jci140989.

STAR★METHODS

KEY RESOURCES TABLE

REAGENT or RESOURCE	SOURCE	IDENTIFIER
Antibodies		
ANGPTL4	Abcam	Cat# ab196746
CD36 for Western blot	Proteintech	Cat# 18836-1-AP; RRID: AB_10597244
NR2F1	Cell Signaling Technology	Cat# 6364T
P27	Proteintech	Cat# 25614-1-AP; RRID: AB_2880161
P21	ABclonal	Cat# AC026; RRID: AB_2768234
PPARγ	WANLEIBIO	Cat# WL01800; RRID: AB_3665462
β-actin	ABclonal	Cat# A19094
HRP-conjugated Rabbit anti-Goat IgG (H+L)	ABclonal	Cat# AS029
TRAP	Santa Cruz	Cat# sc376875; RRID: AB_3075340
Ki-67 for Immunofluorescence Staining	Proteintech	Cat# 27309-1-AP; RRID: AB_2756525
Ki-67 for Tissue Multiplex Immunofluorescence Staining	Aifang Biological	Cat# AF02778
CK7	Aifang Biological	Cat# AF10704
Cy3-conjugated Goat anti-Rabbit IgG (H+L)	ABclonal	Cat# AS007
FITC-conjugated Goat anti-Rabbit IgG (H+L)	ABclonal	Cat# AS011
CD36 for Tissue Multiplex Immunofluorescence Staining	WANLEIBIO	Cat# WL02390; RRID: AB_3668969
Biological samples		
Human serum samples	Shanghai Sixth People's Hospital	N/A
Human pathology tissues	Shanghai Sixth People's Hospital	N/A
Tibia and femur tissue of mice	This paper	N/A
Mouse serum samples	This paper	N/A
Chemicals, peptides, and recombinant proteins		
SSO	MCE	Cat# HY-112847
TRIzol	Invitrogen	Cat# 15596026
sRANKL	Novoprotein	Cat# CJ94
GW9662	MCE	Cat# HY-16578
BW 755C	MCE	Cat# HY-119671
AA	MCE	Cat# HY-109590
EPA	MCE	Cat# HY-B0660
Critical commercial assays		
Mouse AA ELISA Kit	Aifang Biological	Cat# AF30109
Human AA ELISA Kit	Aifang Biological	Cat# AF1466
Human ANGPTL4 ELISA Kit	Aifang Biological	Cat# AF1752
Cell Cycle and Apoptosis Analysis Kit	Beyotime	Cat# C1052
Experimental models: Cell lines		
A549	Zhongqiao Xinzhou	ZQ0003

(*Continued on next page*)

Continued

REAGENT or RESOURCE	SOURCE	IDENTIFIER
H1975	Stem Cell Bank of the Chinese Academy of Sciences	SCSP-597
A549-LUC-GFP	Zhongqiao Xinzhou	LG0001
RAW264.7	Procell	ZQ0003
Oligonucleotides		
Primers for ANGPTL4 and β-actin, see Table S1	Sangon Biotech	N/A
shRNA sequence, see Table S2	HANBIO	N/A
Software and algorithms		
Prism 9.3 software	GraphPad	https://www.graphpad.com/
SPSS software version 22.0	IBM	https://www.ibm.com/cn-zh/spss
Adobe Illustrator	Adobe	https://www.adobe.com/
Flowjo	BD	https://www.flowjo.com/
ImageJ	National Institutes of Health	https://imagej.nih.gov/ij
R	The R foundation	https://www.r-project.org/
HTSeq	Github	https://github.com/htseq/htseq
DEXseq	Github	https://github.com/vivekbhr/Subread_to_DEXSeq
Deposited data		
RNA-seq datasets of dormant A549 cells and osteoclast-activated A549 cells	Gene Expression Omnibus (GEO)	GEO: GSE289262
Other		
PVDF membranes	Millipore	Cat# ISEQ00010
Osteoclasts Culture Kit - For Raw264.7 Cells	Amizona	Cat# AMK2001
Matrigel	Corning	Cat# 354234

EXPERIMENTAL MODEL AND STUDY PARTICIPANT DETAILS

Patients and sample collection

Serum samples (n=143) and pathology samples (n=9) were collected from Shanghai Sixth People's Hospital, affiliated with Shanghai Jiao Tong University, between 2022 and 2023. The study protocol was in accordance with the ethical guidelines set by the Ethics Review Committee of Shanghai Sixth People's Hospital (YS-2019-068). Informed consent was obtained from all subjects. LUAD patients were stratified into primary tumor (n=34) and metastatic groups (n=89) based on pathological confirmation. Metastatic cases were further classified as bone metastases (n=58) or other metastases (n=31) through imaging and histopathological evaluation. Healthy controls (n=20) were age- and sex-matched volunteers with no history of cancer. Serum was collected after centrifugation at 3000 rpm for 5 minutes, followed by centrifugation at 13000 rpm for 10 minutes to collect the supernatant, which was stored at -80°C. Pathology samples included 3 pairs of primary LUAD and bone metastasis specimens. Paraffin-embedded samples were processed to generate serial tumor slides for immunohistochemistry (IHC) staining. Patient information is listed in Table S1. All patients who provided samples were confirmed by pathological examination without preoperative chemoradiotherapy. All patients were from China. The gender and age of the patients did not have a significant influence on the study.

Animal experiments

The animal experiment was approved by the Animal Ethics Committee of Shanghai Sixth People's Hospital. (No: 2019-0355).

To establish a dormant bone metastasis model, 12 female BALB/c nude mice (6-8 weeks old, 20-22g) were purchased from SiPeiFu Biotechnology. Mice were randomly divided into two groups, with six mice in each group. Mice were anesthetized with 1% sodium pentobarbital gas at a dose of 8mL/kg. Dormant A549-GFP-Luc cells were resuspended in 100 μL phosphate-buffered saline (PBS) at a concentration of 1×10^6 cells and injected into the tibia of the mice. After injection, the mice were maintained under specific pathogen-free conditions, and injected PBS or sRANKL at 1/2/3 days after tibia injection. Bioluminescence imaging was performed on the fourth day.

To establish a LUAD bone metastasis model, 6 female BALB/c nude mice (6-8 weeks old, 20-22g) were purchased from SiPeiFu Biotechnology. Mice were anesthetized with 1% sodium pentobarbital gas at a dose of 8mL/kg. A549-GFP-Luc cells were resuspended in 100 μL phosphate-buffered saline (PBS) at a concentration of 1×10^6 cells and injected into the left ventricle of the

mice. After injection, the mice were maintained under specific pathogen-free conditions, and tumor metastasis was assessed by bioluminescence imaging 35 days later. All mice were euthanized with an overdose of isoflurane to minimize discomfort. The sex of the mice had no significant effect on the study results.

METHOD DETAILS

Bioinformatics analysis

The TCGA database (https://tcga-data.nci.nih.gov/tcga) was used for bioinformatic analyses. Gene correlation analysis was performed using Home-for-Researchers Analysis software (https://www.home-for-researchers.com).

Transcriptome sequencing

Dormant A549 cells and osteoclast-activated A549 cells (1×10^6) were collected, lysed, and RNA extracted. RNA was sent to OE Biotech (Shanghai) for sequencing. RNA quality control was performed using the Agilent 2100 Bioanalyzer, with RNA integrity number (RIN) used to assess RNA integrity and quality. High-quality RNA samples with RIN >7 were selected, rRNA-depleted using VAHTS mRNA Capture Beads, and transcriptome libraries were constructed using the VAHTS Universal V5 RNA-seq Library Prep Kit. Library quality and effective concentration were confirmed before performing Illumina sequencing. Raw data were pre-processed using FastQC software to obtain high-quality clean reads for subsequent analysis. Clean reads were aligned to the reference genome using HISAT2 software to obtain read alignment information and gene expression levels (FPKM) for each sample. Read counts for each gene were obtained using HTSeq-count software. Differentially expressed genes (DEGs) were identified using DESeq2 software, with multiple testing corrections applied to calculate q-values. DEGs were filtered using criteria of $|\log2FoldChange|>1$ and q-value<0.05. Hierarchical clustering of DEGs was performed using R software to display gene expression patterns across different groups and samples. Metabolic gene sets were derived from MSigDB and the Kyoto Encyclopedia of Genes and Genomes (KEGG). Volcano plots and heatmaps for the top 20 genes were generated using the R package ggradar.

Construction of 3D dormancy model

Matrigel (354234, Corning) was thawed overnight at 4°C and kept on ice on the day of the experiment. 1×10^5 A549 cells or H1975 cells were resuspended in 800 μL of culture medium and mixed with 200 μL of Matrigel. The mixture was placed in pre-warmed 6-well plates and incubated at 37°C for 1h to allow complete polymerization of the Matrigel. After polymerization, 1 mL of culture medium was added to each well, and the cells were cultured for 48 hours to induce dormancy.

Osteoclast differentiation

RAW264.7 cells (3×10^4) were seeded into each well of a 12-well plate and cultured in the specific medium. Osteoclast differentiation was induced according to the manufacturer's instructions (AMK2001, Amizona), with the medium changed every two days. Mature osteoclasts were stained for tartrate-resistant acid phosphatase (TRAP) using the staining reagent in the kit to confirm successful induction. Conditioned medium (CM) was collected from wells containing mature osteoclasts and RAW264.7 cells, centrifuged at 1500 × g for 10 minutes to remove insoluble debris, and mixed 1:1 with normal culture medium for use.

Cell culture and transfection

A549 and A549-LUC-GFP cells were purchased from Zhongqiao Xinzhou, and H1975 cells were kindly provided by the Stem Cell Bank of the Chinese Academy of Sciences. A549 cells were cultured in DMEM medium (Gibco) supplemented with 10% fetal bovine serum (FBS, EXCELL). A549-LUC-GFP cells were cultured in F12K/DMEM medium (Gibco) supplemented with 10% FBS (EXCELL). H1975 cells were cultured in RPMI-1640 medium (Gibco) supplemented with 10% FBS (EXCELL). RAW264.7 cells were obtained from Procell and cultured in a specific medium (catalog# CM-0190, Procell). All cells were incubated at 37°C in a humidified incubator containing 5% CO_2. All cell lines were authenticated using STR profiling, and all experiments were conducted using mycoplasma-free cells.

Short hairpin RNA (shRNA) vectors were constructed to knock down ANGPTL4 in A549 and H1975 cells. The pcDNA3.1 plasmid vector and the corresponding negative controls was obtained from HanHeng. The specific oligonucleotide sequences are listed in the Table S1. A549 or H1975 cells were seeded into 6-well plates (2×10^5 cells/well). Cells were transfected with shANGPTL4 plasmid using Lipofectamine 3000 (Thermo Fisher Scientific) and Opti-MEM serum-free medium (Gibco) according to the manufacturer's instructions. After 6 hours, the medium was replaced with complete 1640 medium. After 48 hours, cells were treated with 2 μg/mL puromycin in complete 1640 medium to select stable knockdown clones. Protein was collected 3 days later, and knockdown efficiency was verified by Western blot.

Quantitative real-time PCR (qRT-PCR) assay

Total RNA was extracted from cells using TRIzol (Invitrogen) according to the manufacturer's instructions. Reverse transcription and quantitative PCR were performed following the manufacturer's protocol (EZBioscience). The procedure of real-time PCR was described as follows: 95°C for 5 min; 45 cycles of 95°C for 15 s and 60°C for 30 s; 95°C for 15 s, 60°C for 1 min and 95°C for 3 min. Primer sequences for mRNA detection are listed in the supplementary table. Specific PCR primers of ANGPTL4 and β-actin

were purchased from Sangon Biotech, and all qPCR assays were conducted in triplicate. Relative expression of the target gene was normalized to the β-actin mRNA level.

Western blot

Total cell lysates were collected using RIPA, and 15 μg protein was subjected to electrophoresis. Proteins were denatured by heating, subjected to SDS-PAGE, and transferred to PVDF membranes (Millipore) at 350 mA at 4°C for 1.5h. The membranes were blocked with 5% BSA at room temperature for 1 hour and then incubated overnight with primary antibodies. The primary antibodies used were ANGPTL4 (1:2000, ab196746, Abcam), CD36 (1:1000, 18836-1-AP, Proteintech), NR2F1 (1:1000, 6364T, Cell Signaling Technology), P27 (1:1000, 25614-1-AP, Proteintech), P21 (1:1000, A19094, ABclonal), β-actin (1:50000, AC026, ABclonal), and PPARγ (1:1000, WL01800, WANLEIBIO). Secondary antibodies were anti-rabbit (1:10000, AS029, ABclonal). Chemiluminescent signals were detected using ECL substrate (yamei). Image quantification was performed using ImageJ software (NIH).

IHC staining

For IHC staining, antigen retrieval was performed using citrate buffer (pH 6.0). Sections were incubated with primary antibodies (ANGPTL4, 1:200, AB196746, Abcam) overnight at 4°C, followed by incubation with HRP-conjugated rabbit secondary antibodies at room temperature for 1 hour. DAB substrate was used as the chromogen, and hematoxylin was used for counterstaining. Sections were then dehydrated and mounted.

ELISA

Before using serum samples, they were thawed at room temperature and mixed by vortexing. Samples were centrifuged at 13000 rpm for 10 minutes, and the supernatant was collected for ELISA analysis. ELISA was performed according to the manufacturer's instructions (Mouse AA, AF30109-A; Human AA, AF1466-A; Human ANGPTL4, AF-1752-A).

Flow cytometric analysis

Cells were collected and stained with PI (Beyotime, C1052) at 37°C for 30 min, followed by flow cytometric analysis using a Beckman CtoFLEX S. Data were analyzed using Beckman CtoFLEX S software and FlowJo software v10 (FlowJo).

Immunofluorescence staining

Cells (1 × 10^5) were seeded on sterile glass coverslips in 12-well plates and treated as indicated for 2-3 days. Cells were washed with cold PBS, fixed with 4% paraformaldehyde for 10 minutes, and permeabilized with 0.1% Triton X-100 for 10 minutes. Cells were then blocked with PBS containing 1% BSA for 1 hour and incubated overnight at 4°C with primary antibodies (CD36, 1:400; Ki-67, 1:400), followed by incubation with secondary antibodies (cy3,1:200; FITC,1:200) at 4°C for 1 hour in the dark. DAPI (20 mg/ml) labeled the cell nuclei.

Tissue multiplex immunofluorescence staining

After euthanizing the mice, tibiae were extracted and fixed in 10% neutral formalin. Bones were decalcified for 4 weeks in 10% EDTA solution. The bones were then embedded in paraffin and sent to Aifang Bio for multiplex immunofluorescence staining, using specified primary (CK7,1:200, AF10704; CD36, 1:200, WL02390; TRAP, 1:200, sc376875; ANGPTL4, 1:400, ab196746; Ki-67, 1:400, AF02778) and secondary antibodies.

QUANTIFICATION AND STATISTICAL ANALYSIS

Unless otherwise stated, data presented in this study are from at least three independent experiments yielding consistent results. Data are presented as mean ± standard deviation (SD). Statistical analyses were performed using Prism 9.3 software (GraphPad) and SPSS software version 22.0 (IBM). Detailed statistical methods, specific statistical data, and number of biological units are provided in Table S4. The "Number of biological units" refers to the count of independent biological entities in an experiment, such as cell culture replicates, individual animals, or clinical samples, ensuring reliability and variability assessment. A p-value of <0.05 was considered statistically significant.

ADDITIONAL RESOURCES

Clinical samples of this study were obtained from diagnosed LUAD patients, and the study protocol was in accordance with the ethical guidelines set by the Ethics Review Committee of Shanghai Sixth People's Hospital (YS-2019-068). The animal experiment was approved by the Animal Ethics Committee of Shanghai Sixth People's Hospital (No: 2019-0355).